Impact of Fiber Birefringence on Optical Switching With Nonlinear Optical Loop Mirrors

Qiang Lin and Govind P. Agrawal, *Fellow, IEEE*

***Abstract*—We use a vector theory of cross-phase modulation to discuss how residual birefringence of the fiber loop affects the switching performance of a nonlinear optical loop mirror. It is found that the interaction between polarization-mode dispersion (PMD) and cross-phase modulation transfers spatial randomness of residual birefringence to temporal power fluctuations within the switching window. PMD reduces the switching contrast and the reduction depends on wavelength separation between the signal and control pulses as well as on the magnitude of the PMD parameter. Fluctuations in the switched power become worse for a wavelength separation for which the PMD diffusion length associated with birefringence fluctuations becomes comparable to the nonlinear length associated with cross-phase modulation.**

***Index Terms*—Cross-phase modulation (XPM), nonlinear optical loop mirror (NOLM), optical fibers, optical switching, polarization-mode dispersion.**

I. Introduction

CROSS-PHASE modulation (XPM) inside a nonlinear optical loop mirror (NOLM) is used often for ultrafast optical switching [1]–[6]. It has been noted in several experiments that the performance of a NOLM is significantly affected by the residual birefringence of optical fiber used to make the Sagnac loop [7]–[10] if a polarization-maintaining fiber is not used. Residual birefringence was indeed used as a method to reduce the polarization dependence of optical switching [11]. Physically, residual birefringence of optical fibers randomizes the state of polarization (SOP) of both the signal and control pulses and induces differential polarization variations between them through polarization-mode dispersion (PMD) when the two have different carrier frequencies. Since the XPM process responsible for optical switching is polarization dependent [12], PMD induces considerable random variations in the NOLM output. This impact of PMD on optical switching becomes a serious issue for practical implementation of such optical switches.

The scalar theory commonly used for describing NOLM operation [12] cannot include the polarization effects. We have recently developed a vector theory of XPM and have used it to study the combined effects of PMD and XPM on the performance of lightwave systems [13]. In this paper, we use the same approach for studying the effects of PMD on optical switching in NOLMs and show that PMD not only affects the switching window of such devices but also induces considerable fluctuations in the shape, width, and energy of switched pulses. We quantify these fluctuations by solving the underlying equations analytically after appropriate simplifications and compare them with full numerical simulations.

Manuscript received December 31, 2003; revised July 29, 2004. This work is supported in part by the US National Science Foundation under Grant ECS-0320816 and Grant ECS-0334982.

The authors are with the Institute of Optics, University of Rochester, Rochester, NY 14627 USA (e-mail: linq@optics.rochester.edu).

Digital Object Identifier 10.1109/JSTQE.2004.836024

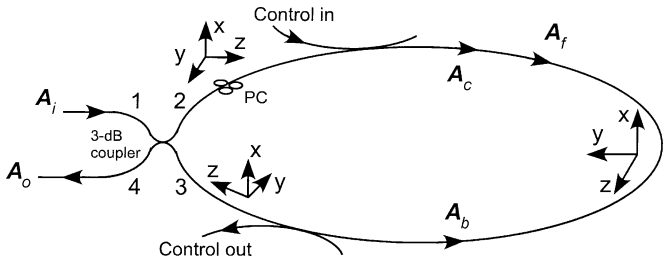

Fig. 1. Notation used for describing optical switching in a NOLM. PC stands for polarization controller.

II. Theoretical Model

Fig. 1 shows a NOLM schematically and the notation used. The input field A_i splits after the polarization-independent 3-dB coupler into forward (clockwise) and backward (counterclockwise) components denoted as $A_f(z,t)$ and $A_b(z,t)$ at a distance z inside the loop. An intense control pulse at a different wavelength is injected after the coupler. It introduces different XPM-induced phase shifts on A_f and A_b as it propagates only in the forward direction. The two signal components interfere at the 3-dB coupler after one round trip. The loop transmissivity depends on the relative phase shift induced by XPM and becomes 100% for a π phase shift provided both pulses maintain their SOP along the same direction.

To include the polarization effects, we express all optical fields by a Jones vector, denoted by $|A_j\rangle$, where the subscript $j = f$, b, or c. This notation is used often for discussing the PMD effects [14]. Using the general form of the nonlinear polarization for silica glass [12] and following the method used earlier in [13], [15], we obtain the following set of three vector equations governing the propagation of three optical fields inside the NOLM:

$$\frac{\partial|A_c\rangle}{\partial z}+\frac{1}{v_c}\frac{\partial|A_c\rangle}{\partial t} = -\frac{i}{2}\omega_c \boldsymbol{B}\cdot\boldsymbol{\sigma}|A_c\rangle + \frac{i\gamma}{3}\left[2\langle A_c|A_c\rangle + |A_c^*\rangle\langle A_c^*|\right]|A_c\rangle \quad (1)$$

$$\frac{\partial|A_f\rangle}{\partial z}+\frac{1}{v_s}\frac{\partial|A_f\rangle}{\partial t} = -\frac{i}{2}\omega_s \boldsymbol{B}\cdot\boldsymbol{\sigma}|A_f\rangle + \frac{2i\gamma}{3}\left[\langle A_c|A_c\rangle + |A_c\rangle\langle A_c| + |A_c^*\rangle\langle A_c^*|\right]|A_f\rangle \quad (2)$$

$$-\frac{\partial|A_b\rangle}{\partial z}+\frac{1}{v_s}\frac{\partial|A_b\rangle}{\partial t}$$
$$=-\frac{i}{2}\omega_s\boldsymbol{B}\cdot\boldsymbol{\sigma}|A_b\rangle$$
$$+\frac{2i\gamma}{3}\left[\langle A_c|A_c\rangle+|A_c\rangle\langle A_c|+|A_c^*\rangle\langle A_c^*|\right]|A_b\rangle \quad (3)$$

where ω_j and $v_j (j = c, s)$ are the carrier frequency and the group velocity for the control and signal pulses, respectively. The nonlinear parameter γ is taken to be nearly the same for the two waves assuming that their frequency difference $|\omega_s - \omega_c|$ is relatively small compared with the carrier frequencies themselves. $\langle A|$ and $|A^*\rangle$ are Hermitian and complex conjugate of $|A\rangle$, respectively.

The main approximation made in deriving (1)–(3) is that the control pulse is assumed to be much more intense than signal pulses. Thus, self-phase modulation (SPM) and XPM induced by the control pulse are included but those induced by the signal pulse are neglected because of its weak nature. Fiber losses are neglected because the length of the loop is typically only a few kilometers. The effects of group-velocity dispersion (GVD) are also ignored assuming that pulses are wide enough that dispersion length exceeds the loop length considerably. To solve (1)–(3), we make one more simplification. In practice, the XPM effects on the backward field $|A_b\rangle$ induced by the control pulse are so small because of the counterpropagating nature of two pulses (walkoff length $\sim$1 cm even for a 100-ps pulse) that we can ignore them. The backward propagating field $|A_b\rangle$ is then only affected by fiber birefringence, and (3) can be solved analytically after setting $\gamma = 0$.

Residual birefringence of the fiber enters through the three-dimensional (3-D) vector $\boldsymbol{B}$. This vector is written in the Stokes space using the spin vector $\boldsymbol{\sigma}$, whose three components represent the three Pauli matrices [14]. Because of the counterpropagating nature of the two signal pulses [16], [17], the Jones matrices associated with birefringence-induced SOP evolution for $|A_f\rangle$ and $|A_b\rangle$ are $\overleftrightarrow{\mathbf{T}}$, and $\overleftrightarrow{\mathbf{T}}^t$, respectively, where $\overleftrightarrow{\mathbf{T}}^t$ is the transpose of $\overleftrightarrow{\mathbf{T}}$, and $\overleftrightarrow{\mathbf{T}}$ is the solution of $d\,\overleftrightarrow{\mathbf{T}}/dz = -(i/2)\omega_s\boldsymbol{B}\cdot\boldsymbol{\sigma}\,\overleftrightarrow{\mathbf{T}}$. The solution of (3) can now be used to write $|A_b\rangle$ at port 2 after one round trip as

$$|A_b(0,t)\rangle = \overleftrightarrow{\mathbf{T}}^t(L)\left|A_b\left(L, t-\frac{L}{v_s}\right)\right\rangle$$
$$= \frac{i\,\overleftrightarrow{\mathbf{T}}^t(L)\sigma_1\left|A_i\left(t-\frac{L}{v_s}\right)\right\rangle}{\sqrt{2}} \quad (4)$$

where $|A_i\rangle$ is the input field at port 1 and σ_1 is one of the Pauli matrices [14]. The factor of $i/\sqrt{2}$ results from the transfer matrix of a 3-dB coupler, which not only splits the power into half but also introduces a $\pi/2$ phase shift [4]. The origin of σ_1 matrix lies in the fact that we are working in a reference frame associated with the forward-propagating pulse that flips its y-axis after a round trip (see Fig. 1). It is also useful to introduce a retarded time in this frame as $\tau = t - z/v_s$.

The NOLM output at port 4 corresponds to the switched pulse. The power profile of this pulse is obtained by interfering the two counterpropagating field components at the 3-dB coupler and is given by

$$P_o(\tau) = \frac{\{P_i(\tau) - \mathrm{Re}\,[\rho_0(L,\tau)]\}}{2} \quad (5)$$

where Re denotes the real part, $P_i(\tau) = \langle A_i(\tau)|A_i(\tau)\rangle$ is the input pulse profile at port 1 of the coupler, and the scalar quantity ρ_0 describes the interference effects and is defined as

$$\rho_0(z,\tau) = \left\langle A_i(\tau)\left|\sigma_1\,\overleftrightarrow{\mathbf{T}}^*(L)\sigma_1\,\overleftrightarrow{\mathbf{T}}(L)\right|A_f'(z,\tau)\right\rangle \quad (6)$$

where $\overleftrightarrow{\mathbf{T}}^*$ is the complex conjugate of $\overleftrightarrow{\mathbf{T}}$ and we used the relation $|A_f(z,\tau)\rangle = \overleftrightarrow{\mathbf{T}}(z)|A_f'(z,\tau)\rangle$ since $|A_f'(z,\tau)\rangle$ is only affected by the XPM from the control pulse; it would remain constant in the absence of the XPM effects. All birefringence-induced polarization effects are included through the random quantity ρ_0.

Residual birefringence affects the NOLM output in two ways. First, it randomizes the SOPs of the control and signal pulses along the fiber and, thus, affects the XPM process locally. Second, because of the interferometric nature of the NOLM, SOP variations affect the output even in the absence of any control pulse [16], [17]. To optimize the performance, a polarization controller is adjusted inside the loop such that P_o is minimum in the absence of control pulses. Mathematically, this is equivalent to setting $\sigma_1\,\overleftrightarrow{\mathbf{T}}^*\,\sigma_1\,\overleftrightarrow{\mathbf{T}} = \sigma_0$ [18], where σ_0 is a unit matrix and $\overleftrightarrow{\mathbf{T}}$ includes the SOP rotation induced by the polarization controller. If residual birefringence varies with time because of environmental perturbations, $\overleftrightarrow{\mathbf{T}}$ also changes randomly on a time scale associated with birefringence fluctuations. We assume that optimization is maintained by adjusting the polarization controller adaptively and focus only on the PMD effects on XPM inside the NOLM. The quantity ρ_0 is then given by $\rho_0(z,\tau) = \langle A_i(\tau)|A_f'(z,\tau)\rangle$ and does not require knowledge of the matrix $\overleftrightarrow{\mathbf{T}}(L)$.

III. XPM-Induced Switching

To calculate ρ_0, we need the field $|A_f'(L,\tau)\rangle$ after its phase has been affected by the control pulse through XPM. However, the XPM effects are nonuniform within the loop because PMD changes the relative SOP of the control pulse with respect to the signal pulse in a random fashion. Moreover, SPM and XPM also affect the SOPs of the two pulses through a phenomenon known as nonlinear polarization rotation (NPR). One can simplify the analysis by noting that both the beat length and the correlation length associated with residual birefringence are $\sim$10 m for spooled fibers [19], [28] and are much shorter than typical nonlinear lengths ($\sim$1 km). Rapid SOP variations induced by $\overleftrightarrow{\mathbf{T}}(z)$ thus average over the nonlinear effects, leading to a reduced nonlinear parameter defined as $\gamma_e = 8\gamma/9$ [20]. After this averaging, $|A_f'(z,\tau)\rangle$ and $|A_c'(z,\tau)\rangle = \overleftrightarrow{\mathbf{T}}^{-1}(z)|A_c(z,\tau)\rangle$ evolve inside the loop as [13]

$$\frac{\partial|A_f'\rangle}{\partial z} = \frac{i\gamma_e}{2}P_c(z,\tau)(3+\hat{p}\cdot\boldsymbol{\sigma})|A_f'\rangle \quad (7)$$

$$\frac{\partial|A_c'\rangle}{\partial z}+\delta\beta_1\frac{\partial|A_c'\rangle}{\partial\tau} = -\frac{i}{2}\Omega\mathbf{b}\cdot\boldsymbol{\sigma}|A_c'\rangle+i\gamma_e P_c(z,\tau)|A_c'\rangle \quad (8)$$

where $\Omega = \omega_c - \omega_s$ is the carrier frequency difference between the two pulses and $\delta\beta_1 = 1/v_c - 1/v_s$ describes their group-velocity mismatch. The birefringence vector $\boldsymbol{b}(z)$ is related to $\boldsymbol{B}(z)$ by a rotation in the Stokes space corresponding to $\overleftrightarrow{\mathbf{T}}(z)$.

Equations (7) and (8) show that both the power P_c and the SOP $\hat{p}$ of the control pulse affect the XPM-induced phase shift. The power of the control pulse is given by $P_c(z,\tau) = \langle A_c'|A_c'\rangle = \langle A_c|A_c\rangle$. Its SOP is governed by the unit vector $\hat{p}(z,\tau) = \langle A_c'|\boldsymbol{\sigma}|A_c'\rangle/P_c$, representing the direction of its Stokes vector on the Poincaré sphere. Both the control and signal pulses maintain their shape inside the NOLM (assuming negligible dispersion-induced pulse broadening) although two pulses walk away from each other because of group-velocity mismatch. Thus, $P_c(z,\tau) = P_c(0,\tau - \delta\beta_1 z)$ in (7) and (8). This feature simplifies the following analysis considerably.

The output power P_o of the switched pulse is determined by the interference term ρ_0. We use its expression together with (7) and (8) to arrive at the following set of three closed equations:

$$\frac{\partial\rho_0}{\partial z} = \frac{i\gamma_e P_c}{2}(3\rho_0 + \hat{p}\cdot\boldsymbol{\rho}) \tag{9}$$

$$\frac{\partial\boldsymbol{\rho}}{\partial z} = \frac{i\gamma_e P_c}{2}(3\boldsymbol{\rho} + \rho_0\hat{p}) - \frac{\gamma_e}{2}P_c\hat{p}\times\boldsymbol{\rho} \tag{10}$$

$$\frac{\partial\hat{p}}{\partial z} = \Omega\boldsymbol{b}\times\hat{p} \tag{11}$$

where the vector $\boldsymbol{\rho}$ is introduced as $\boldsymbol{\rho}(z,\tau) = \langle A_i(\tau)|\boldsymbol{\sigma}|A_f'(z,\tau)\rangle$. Notice that both ρ_0 and $\boldsymbol{\rho}$ are complex quantities and related through the identities $\rho_0^2 = \boldsymbol{\rho}^2$ and $|\rho_0|^2 + |\boldsymbol{\rho}|^2 = 2P_i^2$.

Equations (9)–(11) are three linear stochastic equations and can be easily solved numerically to find ρ_0 and then calculate transmitted power $P_o(\tau)$ for given temporal profiles, $P_i(\tau)$ and $P_c(0,\tau)$, for the input and control pulses, respectively. Since fiber length is typically much longer than the correlation length associated with birefringence fluctuations, we model $\boldsymbol{b}$ as a 3-D Markovian Gaussian process whose first- and second-order moments are given by [21], [22]

$$\overline{\mathbf{b}(z)} = 0, \qquad \overline{\mathbf{b}(z_1)\mathbf{b}(z_2)} = \left(\frac{D_p^2}{3}\right)\overleftrightarrow{\mathbf{I}}\,\delta(z_2 - z_1) \tag{12}$$

where an overbar denotes average over a birefringence ensemble, $\overleftrightarrow{\mathbf{I}}$ is the 3-D unit matrix, and D_p is the PMD parameter of the fiber.

To show the effects of PMD on the switching window of an NOLM, we consider a 3-km-long NOLM with $\gamma = 2\mathrm{W}^{-1}/\mathrm{km}$, $D_p = 0.1$ ps/$\sqrt{\mathrm{km}}$, $\beta_3 = 0.1$ ps^3/km, and a zero-dispersion wavelength (ZDWL) of $\lambda_0 = 1550$ nm. The power of the Gaussian-shape control pulse at 1545 nm varies as $P_c(0,\tau) = P_0\exp(-\tau^2/T_0^2)$, where $T_0 = 10$ ps and peak power $P_0 = 820$ mW. The signal is assumed to have a continuum-wave (CW) form at a wavelength of 1575 nm. The switching window is defined as the loop transmissivity as $P_o(\tau)/P_i(\tau)$. The 30-nm wavelength difference between the signal and control waves introduces considerable walk off between the two and produces a nearly rectangular 40-ps switching window shown by the dotted line in Fig. 2 when fiber has no birefringence (the ideal case). When residual birefringence is included by choosing $D_p = 0.1$ ps/$\sqrt{\mathrm{km}}$ and

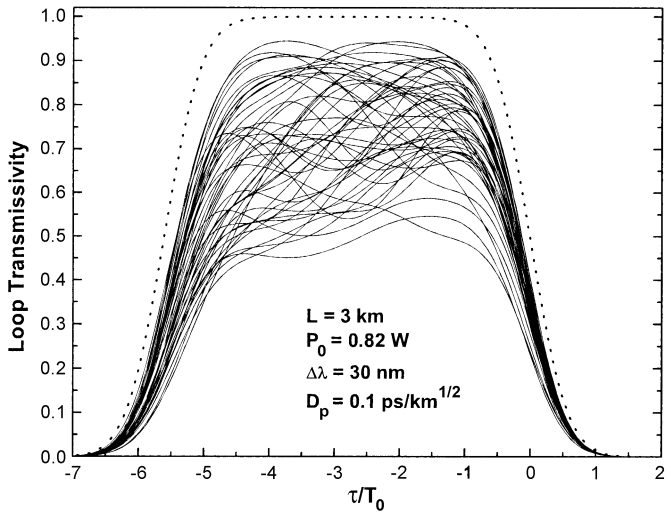

Fig. 2. Switching windows of a NOLM under the impact of residual birefringence (solid curves) created by a Gaussian-shape control pulse. The dotted curve shows for comparison the switching window in the absence of residual birefringence. For all the curves, the control and signal waves are linearly copolarized at the location where the control pulse is injected into the loop. Parameters are given in the text.

a correlation length of 10 m, the switching window depends on the birefringence distribution along the fiber length and varies for each realization of the stochastic process. Fig. 2 shows some examples of the switching window obtained by solving (1)–(3) numerically, assuming that the signal and control are linearly copolarized at the location where the control is injected to the loop. A comparison of these curves with the dotted curve shows that PMD effects not only reduce the NOLM transmission during switching, but also make the transmissivity to vary with time along the switching window. As a result, switching window become distorted, and the extent of distortion depends on the specific distribution of residual birefringence inside the NOLM. Since this distribution will change from fiber to fiber, different NOLMs made from the same spool of fiber would exhibit quite different switching performances.

One may wonder what makes NOLM transmission to vary randomly within the switching window for a given NOLM if nothing is changing with time. More specifically, if both P_i and P_c are deterministic quantities at any time τ, why P_o fluctuates in a random fashion with τ. From a physical standpoint, this is a consequence of PMD-induced changes in the SOP of various fields and resulting variations in the XPM efficiency. The combination of the two effects produces *intrapulse* depolarization for the signal manifested as a random SOP of the signal along the pulse profile [23]. In effect, spatial randomness of residual birefringence is translated into temporal randomness at the NOLM output by the Sagnac interferometer.

IV. Average Output Power and Fluctuation Level

As seen in Fig. 2, the NOLM output is random in two ways because of PMD. First, if birefringence distribution along the fiber length is frozen and does not change with time, switching window is distorted but is static. The output power then varies along the switching window in a random fashion but does not fluctuate at any given moment. Second, if birefringence distribution along the fiber length changes with time in a dynamic

fashion because of environmental perturbations, the output power at any instant of time itself begins to fluctuate on a time scale associated with such perturbations. Although this time scale is relatively long (ranging from a few seconds to several hours), such random fluctuations in the output of an NOLM are not acceptable in practice. It is thus important to estimate the average and variance of such environment-induced power fluctuations. It turns out that these two moments of the output power can be calculated in a semianalytical fashion.

The average value $\overline{P_o}$ and variance $\sigma_o^2 = \overline{P_o^2} - \overline{P_o}^2$ of the output power are obtained from (5) and are related to the moments of ρ_0 as

$$\overline{P_o}(\tau) = \frac{\{P_i(\tau) - \mathrm{Re}\,[\overline{\rho_0}(L,\tau)]\}}{2} \tag{13}$$

$$\sigma_o^2(\tau) = \frac{\left[\mathrm{Re}(\overline{\rho_0^2} - \overline{\rho_0}^2) + \overline{|\rho_0|^2} - |\overline{\rho_0}|^2\right]}{8}. \tag{14}$$

Although the average value $\overline{P_o}$ does not correspond to a single experimental measurement, it provides a good indication of the PMD effect on the switchiing performance of NOLMs. The evolution equations for $\overline{\rho_0}$, $\overline{\rho_0^2}$, and $\overline{|\rho_0|^2}$ can be obtained from (9)–(11) after averaging over random residual birefringence using a procedure described in [15]. For the mean value of ρ_0, we obtain the following two coupled equations:

$$\frac{\partial\overline{\rho_0}}{\partial z} = \frac{i\gamma_e P_c}{2}(3\overline{\rho_0} + \overline{\hat{p}\cdot\boldsymbol{\rho}}) \tag{15}$$

$$\frac{\partial(\overline{\hat{p}\cdot\boldsymbol{\rho}})}{\partial z} = -\eta(\overline{\hat{p}\cdot\boldsymbol{\rho}}) + \frac{i\gamma_e P_c}{2}(\overline{\rho_0} + 3\overline{\hat{p}\cdot\boldsymbol{\rho}}) \tag{16}$$

where $\eta = 1/L_d = (D_p\Omega)^2/3$ and L_d is the PMD diffusion length of the relative SOP orientation between the two pulses. Note that L_d is not only a function of the PMD parameter of fiber, but also depends on the the carrier frequency separation between the control and signal pulses, which plays an important role on the switching performance.

Following the same procedure, the second-order moment $\overline{\rho_0^2}$ is obtained by solving the following three coupled equations:

$$\frac{\partial\overline{\rho_0^2}}{\partial z} = i\gamma_e P_c(3\overline{\rho_0^2} + U_1) \tag{17}$$

$$\frac{\partial U_1}{\partial z} = (3i\gamma_e P_c - \eta)U_1 + \frac{i\gamma_e P_c}{2}(V_1 + \overline{\rho_0^2}) \tag{18}$$

$$\frac{\partial V_1}{\partial z} = (3i\gamma_e P_c - 3\eta)V_1 + \eta\overline{\rho_0^2} + i\gamma_e P_c U_1 \tag{19}$$

where $U_1 = \overline{\hat{p}\cdot\rho_0\boldsymbol{\rho}}$ and $V_1 = \overline{(\hat{p}\cdot\boldsymbol{\rho})^2}$. Similarly, $\overline{|\rho_0|^2}$ can be obtained by solving

$$\frac{\partial\overline{|\rho_0|^2}}{\partial z} = \gamma_e P_c U_2 \tag{20}$$

$$\frac{\partial U_2}{\partial z} = -\eta U_2 + \gamma_e P_c\left(V_2 - \overline{|\rho_0|^2}\right) \tag{21}$$

$$\frac{\partial V_2}{\partial z} = -3\eta V_2 - \gamma_e P_c U_2 + \eta\left(2P_i^2 - \overline{|\rho_0|^2}\right). \tag{22}$$

where $U_2 = \mathrm{Im}(\overline{\hat{p}\cdot\rho_0\boldsymbol{\rho}^*})$, $V_2 = \overline{|\hat{p}\cdot\boldsymbol{\rho}|^2}$, and Im denotes the imaginary part. All of these deterministic equations can be solved easily on a computer. Analytical solutions can also be obtained in some specific cases.

We first consider the loop transmissivity for a square-shape control pulse when the control and signal wavelengths are tuned symmetrically around the ZDWL so that their group velocities always match. The switching window under such conditions has the same shape and duration as the control pulse. We focus on the same 3-km-long fiber loop used for Fig. 2, but set the control peak power to $P_\pi = 262$ mW, a value that represents the control power for which the entire copolarized signal is transmitted in the absence of residual birefringence when there is no walkoff between the two pulses. Fig. 3(a) shows the average loop transmissivity (or switching contrast) defined as $T_L = \overline{P_o}/P_i$ at the control pulse peak by plotting T_L as a function of signal-control wavelength detuning $\Delta\lambda = |\lambda_s - \lambda_c|$ for three values of the PMD parameter D_p. Fig. 3(b) shows the fluctuation level, defined as σ_o/P_i, under the same conditions. In both cases, solid and dashed curves are respectively for the copolarized and orthogonally polarized control pulse with respect to the signal SOP at the input end. Dotted curves show for comparison the no-birefringence case for these two polarization configurations. The control only imposes a phase shift of $\pi/3$ on the signal when the two are orthogonally polarized, resulting in only 25% transmission in the ideal case (lower dotted line).

To justify the semianalytical theory presented here, we carried out full numerical simulations based on (1)–(3) by dividing the 3-km-long fiber into 10-m-long sections. Birefringence was kept constant inside each section but both its magnitude and axes are changed randomly from section to section. More precisely, the magnitude of birefringence follows a Gaussian distribution with zero mean while the principal axes are rotated uniformly after each section. The results averaged over 300 runs are shown as filled circles in Fig. 3. The semianalytical results agree quite well with the Monte-Carlo numerical simulations. In particular, the predicted average transmissivity almost coincides in the two cases. A small discrepancy seen in the prediction of the fluctuation level comes from the sample size of 300 used for numerical simulations. It decreases as the sample size is increased but only at the expense of a longer computational time.

As seen in Fig. 3(a), residual birefringence of the fiber loop reduces the NOLM transmission considerably on average for copolarized signal and control pulses, thereby degrading the switch performance. When $\Delta\lambda$ is small enough to make PMD diffusion length L_d larger than the NOLM length L, the signal and control nearly maintain their relative SOPs inside the NOLM even though the SOP of each field can change considerably. The switching contrast is then only affected by reduction in γ by a factor of 8/9 and is reduced by a mere 3% for $\Delta\lambda = 1$ or 2 nm. The similar effect in the orthogonally polarized case increases the XPM-induced nonlinear phase from $\pi/3$ to $4\pi/9$, resulting in a loop transmissivity of 41.3%. However, the average switching contrast changes quickly with increase in $\Delta\lambda$ or D_p, as seen in Fig. 3(a). In fact, the NOLM approaches a polarization-independent switching contrast of 75% (corresponding to a nonlinear phase shift of $2\pi/3$) for large wavelength separations such that $L_d \ll L$. These results are qualitatively consistent with the experimental results of

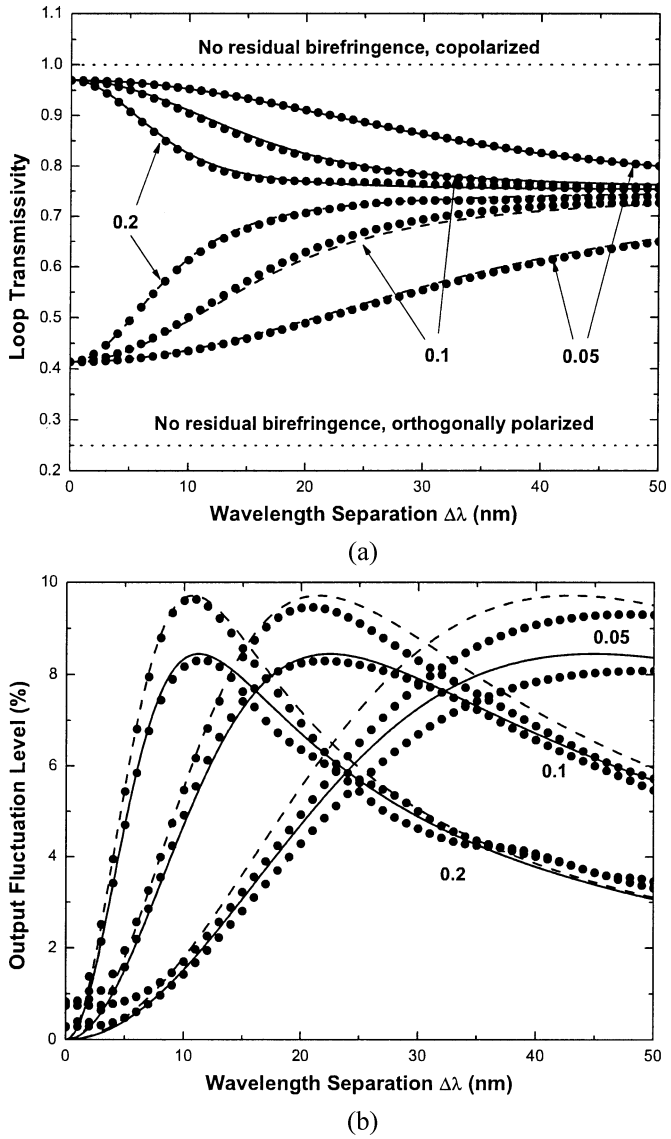

Fig. 3. Switching contrast (a) and fluctuation level of output (b) plotted as a function of wavelength separation between the signal and control for three values of PMD parameter D_p (in units of ps/$\sqrt{\text{km}}$) for the copolarized (solid curves) and orthogonally polarized (dashed curves) cases. Dotted lines show the no-birefringence case for the same two polarization configurations. Filled circles shows the Monte-Carlo simulation results.

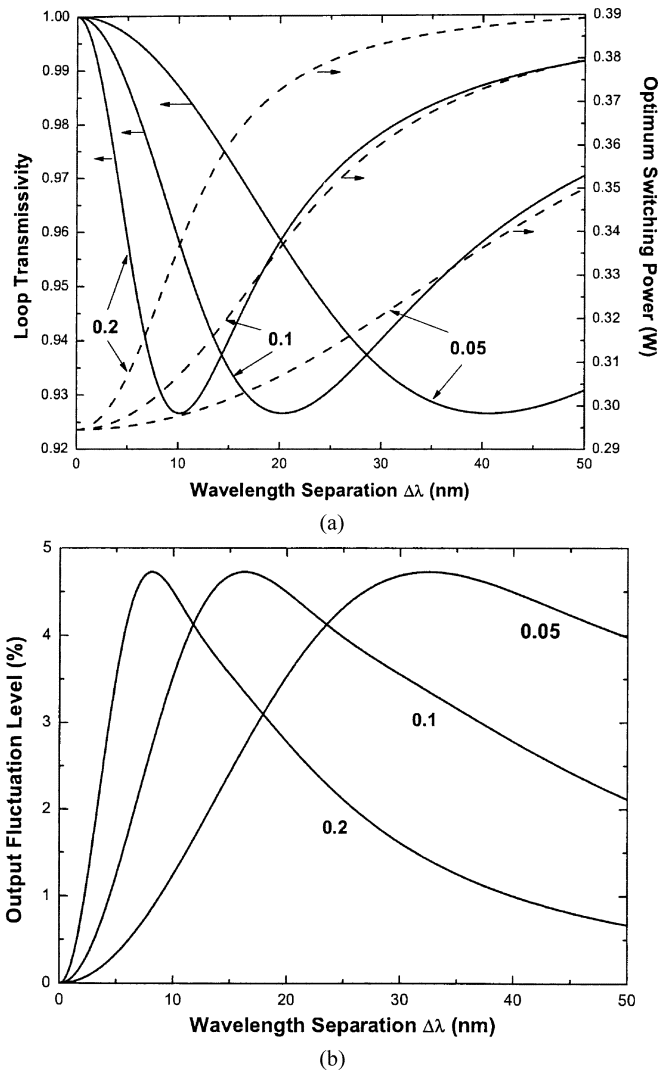

Fig. 4. (a) Maximum switching contrast (solid curves) and optimum control power (dashed curves) as a function of wavelength separation between the signal and control (both linearly copolarized initially) for three values of PMD parameter D_p (in units of ps/$\sqrt{\text{km}}$). (b) Output fluctuation level under the optimum conditions.

[11]. The level of PMD-induced fluctuations depends on the length ratio $\mu = L_n/L_d$, where $L_n = (2\gamma_e P_0)^{-1}$ is the nonlinear length for XPM-induced phase shift. It becomes maximum when $\mu \approx 1$, resulting in a peak value of about 9% in Fig. 3(b). Around the spectral region where $\mu \approx 1$, the NOLM is most susceptible to environmental perturbations. The qualitative behavior is similar for all values of D_p. The only difference is that the peak in Fig. 3(b) shifts to smaller values of $\Delta\lambda$ for larger values of D_p.

The PMD-induced reduction in the switching contrast can be compensated to some extent by increasing the control power P_c. This increase in control power was observed in the experiment of [9]. Of course, the optimum value of power depends on both the wavelength separation $\Delta\lambda$ and the value of the PMD parameter D_p. Moreover, it is not possible to realize 100% switching contrast even with this optimization. The solid and dashed curves in Fig. 4(a) show, respectively, the optimized switching contrast and the control power required for it as a function of $\Delta\lambda$ for copolarized control and signal at the input end. When $\Delta\lambda \approx 0$, the reduction in γ can be overcome by increasing P_π from 262 to 295 mW for complete switching. However, this power level increases to 380 mW for $\Delta\lambda = 50$ nm inside a fiber with $D_p = 0.1$ ps/$\sqrt{\text{km}}$, even if there is no walk off between the two waves. Complete switching with 100% contrast becomes difficult to realize when $\mu \approx 1$. As seen in Fig. 4(a), the optimized switching contrast is close to 92% when μ is close to 1. Fig. 4(b) shows the the fluctuation level under optimum conditions. It is reduced considerably compared with the values seen in Fig. 3(b). Maximum fluctuation level is about 4.5% and occurs again when μ is close to 1.

V. Switching Window

We now consider the temporal switching window and assume that the NOLM output is being switched for a short du-

ration using control pulses of Gaussian shape with $T_0 = 10$ ps and a peak power of 262 mW. The control wavelength of 1545 nm is 5-nm shorter than the 1550-nm ZDWL of the fiber loop. The signal is again in the CW form, but our results also apply for a pulsed signal as long as the signal pulse is much wider than the control pulse. The two waves are linearly copolarized at the location where the control is injected to the loop. The signal wavelength is varied from 1555 to 1575 nm to study the impact of the group-velocity mismatch, whose magnitude can be calculated from the third-order dispersion of the fiber using $\delta\beta_1 = 1/v_c - 1/v_s = \beta_3(\omega_c - \omega_s)(\omega_c + \omega_s - 2\omega_0)/2$, where $\omega_0 = 2\pi c/\lambda_0$ is the zero-dispersion frequency. The fiber is assumed to have a third-order dispersion of $\beta_3 = 0.1\text{ps}^3/\text{km}$ at ZDWL. The GVD-induced pulse broadening can be neglected because the dispersion lengths exceed 50 km in all cases.

Solid curves in Fig. 5(a) show the "averaged" switching window by plotting average value of the NOLM transmissivity $\overline{P_o(\tau)}/P_i(\tau)$ as a function of time for three signal wavelengths separated from the control wavelength by 10, 20, and 30 nm. All NOLM parameters are the same as those used for Fig. 3 except for $D_p = 0.1$ ps/$\sqrt{\text{km}}$. Dotted curves show the switching window in the absence of residual birefringence. The switching window is relatively narrow and has 100% contrast at its peak for $\Delta\lambda = 10$ nm because the walkoff effects disappear when the control and signal wavelengths are located symmetrically around the ZDWL. The walkoff effects broaden the switching window and reduce the transmissivity as $\Delta\lambda$ increases to 20 and 30 nm. The PMD effects make the situation worse because they reduce the transmissivity even further and also make the switching window asymmetric. The asymmetry is related to the fact that control pulse overlaps with different slices of the signal pulse at different locations inside the fiber.

When $\Delta\lambda = 20$ nm, a value for which $\mu \approx 1$, only 60% of signal power can be switched to output port on average and this value drops to below 15% for $\Delta\lambda = 30$ nm. Fig. 5(b) shows the fluctuation level within the switching window under the conditions of Fig. 5(a). The peak fluctuation level is under 5% for $\Delta\lambda = 10$ nm, increases to around 9% for $\Delta\lambda = 20$ nm and then drops to below 3% for $\Delta\lambda = 30$ nm. This behavior is similar to that seen in Fig. 3 but is modified significantly because of the reduction in the XPM effects induced by pulse walkoff. For $D_p = 0.1$ ps/$\sqrt{\text{km}}$, large fluctuations occur for $\Delta\lambda = 20$ nm but are reduced considerably for smaller or larger wavelength separations. Again, the analytical results agree well with the numerical ones based on full Monte-Carlo simulations (filled circles). Note that the fluctuation level depends on the control peak power as well as the loop length. If the control peak power is increased to achieve a maximum peak switching contrast as shown in Fig. 2 for $\Delta\lambda = 30$ nm, the fluctuation level will increase considerably.

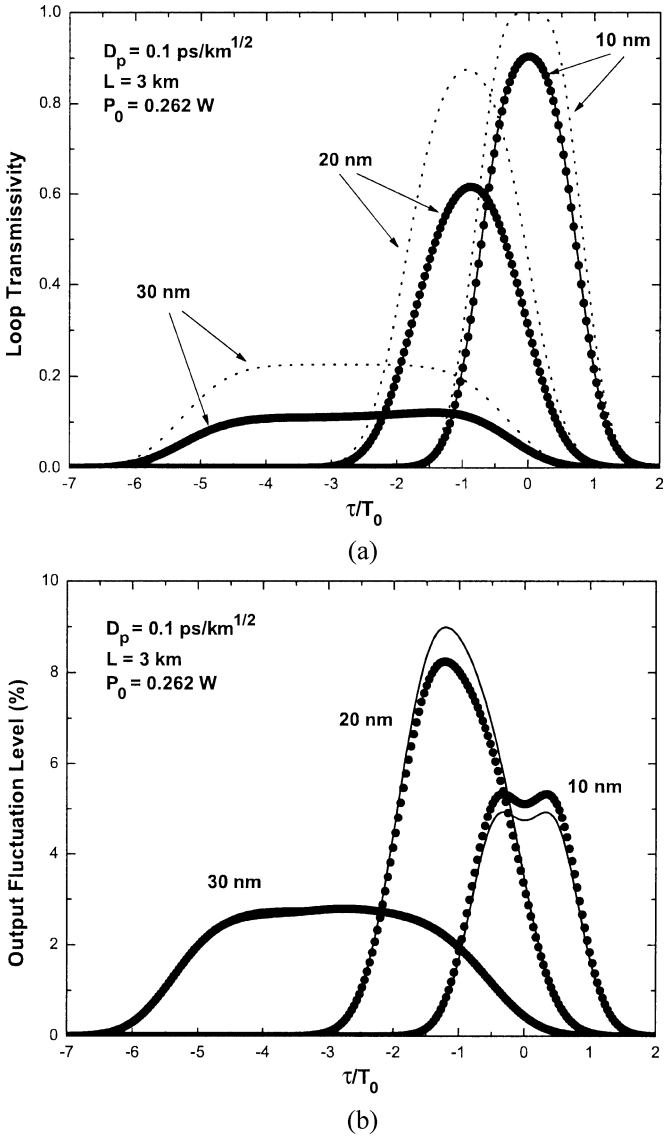

Fig. 5. Switching windows (a) and fluctuation level of output (b) for three values of wavelength separation between the signal and control waves. The control is fixed at 1545 nm, but the signal wavelengths are 1555, 1565, 1575 nm for the three cases, respectively. In each case, NOLM transmissivity is plotted as a function of time for Gaussian-shape control pulses. Solid lines show the analytical results and dotted lines show for comparison the no-birefringence case. Filled circles show the Monte-Carlo simulation results, which overlap with the solid curves in most of the cases.vsk

VI. Conclusion

In this paper, we have presented a vector theory of XPM that is capable of including the PMD effects while describing the switching performance of an NOLM. The interaction between the PMD and XPM phenomena transfers the spatial randomness of residual birefringence to temporal fluctuations on the switched-pulse profile. Physically speaking, the combination of PMD and XPM induces intrapulse depolarization on the signal in the sense that different parts of the signal pulse have different randomly varying SOPs. Because of this depolarization, PMD reduces the switching contrast and the polarization dependence when signal and control wavelengths are chosen to be further apart than a few nanometers. The contrast can be improved to some extent by increasing the control power but it cannot be made 100% in the spectral region where the PMD diffusion length becomes comparable to the nonlinear length. Under environmental perturbations, PMD induced fluctuations on the switched pulse can be up to 9% of the input power, depending on the fiber length and the value of the PMD parameter for that fiber. Our results qualitatively agree with the existing experimental observations [9], [11]. Further experiments would help to verify our predictions.

The use of a polarization-diversity loop has been proposed to reduce the polarization dependence of an NOLM-vased optical switch [10], [24]. Our analysis shows that such a loop cannot mitigate the PMD effects on XPM because of the PMD and XPM effects interact locally all along the loop length. For the same reason, a Faraday mirror inside a folded ultrafast nonlinear interferometer can reduce the effect of global SOP evolution induced by linear birefringence [9], [25] but it cannot eliminate the degradation induced by local interaction between the PMD and XPM. For these reasons, PMD is likely to remain a limiting factor for XPM-based optical switching whenever fiber-loop lengths exceeds a few kilometers. The ultimate solution of this problem relies on the availability of fibers with ultralow PMD and high nonlinearity. Even though the intrinsic nonlinearity of silica, governed by the n_2 parameter, cannot be changed, the nonlinear parameter γ can be enhanced by reducing the effective core area a_{eff} of the fiber since the two are related as $\gamma = 2\pi n_2/(\lambda a_{\text{eff}})$ [12]. A fiber with large values of γ is referred to as a highly nonlinear fiber. An increase in γ by a factor of 8–10 will reduce the loop length of NOLMs to below 400 m and will help to increase the device performance considerably [26], [27].

We should stress that our analytic theory is based on the assumption of a delta-function correlation among residual birefringence fluctuations. We have performed numerical simulations to judge the validity of this approximation by changing the birefringence correlation length l_c. The results shown in Figs. 3–5 change only by a small amount even when l_c is increased up to 100 m. Numerical simulations show that our analytic theory works reasonably well when the NOLM length is 10 to 15 larger than the birefringence correlation length. In the case of highly nonlinear fibers, loop lengths of less than 100 m may be sufficient for optical switching. Similarly, for pulses shorter than a few picoseconds, loop length is generally kept short as $\sim$100 m to prevent pulse broadening. In these cases, residual birefringence fluctuations cannot be treated as delta-correlated (white noise), and a numerical approach should be used. On the other hand, even though it is easy to include numerically pulse broadening induced by GVD and higher-order dispersion, we have not done so since the loop length is generally kept shorter than the dispersion length in almost all practical situations.

REFERENCES

[1] K. J. Blow, N. J. Doran, B. K. Nayar, and B. P. Nelson, "Two-wavelength operation of the nonlinear fiber loop mirror," *Opt. Lett.*, vol. 15, pp. 248–250, 1990.

[2] P. Boffi, L. Marazzi, and M. Martinelli, "A novel interferometric wavelength converter," *IEEE Photon. Technol. Lett.*, vol. 11, pp. 1393–1395, Nov. 1999.

[3] J. Yu, X. Zheng, C. Peucheret, A. T. Clausen, H. N. Poulsen, and P. Jeppesen, "All-optical wavelength conversion of short pulses and NRZ signals based on a nonlinear optical loop mirror," *J. Lightwave Technol.*, vol. 18, pp. 1007–1017, 2000.

[4] G. P. Agrawal, *Applications of Nonlinear Fiber Optics*. San Diego, CA: Academic, 2001, ch. 3.

[5] J. H. Lee, P. C. Teh, P. Petropoulos, M. Ibsen, and D. Richardson, "All-optical modulation and demultiplexing systems with significant timing jitter tolerance through incorporation of pulse-shaping fiber Bragg gratings," *IEEE Photon. Technol. Lett.*, pp. 203–205, 2002.

[6] N. Chi, L. Xu, K. S. Berg, T. Torger, and P. Jeppesen, "All-optical wavelength conversion and multichannel 2R regeneration based on highly nonlinear dispersion-imbalanced loop mirror," *IEEE Photon. Technol. Lett.*, vol. 14, pp. 1581–1583, Nov. 2002.

[7] N. Finlayson, B. K. Nayar, and N. J. Doran, "Switch inversion and polarization sensitivity of the nonlinear-optical loop mirror," *Opt. Lett.*, vol. 17, pp. 112–114, 1992.

[8] M. F. Arend, M. L. Dennis, I. N. Duling III, E. A. Golovchenko, A. N. Pilipetskii, and C. R. Menyuk, "Nonlinear-optical loop mirror demultiplexer using a random birefringence fiber: comparisons between simulations and experiments," *Opt. Lett.*, vol. 22, pp. 886–888, 1997.

[9] C. Vinegoni, M. Wegmuller, B. Huttner, and N. Gisin, "All optical switching in a highly birefringence and a standard telecom fiber using a Faraday mirror stabilization scheme," *Opt. Commun.*, vol. 182, pp. 335–341, 2000.

[10] T. Sakamoto, H. C. Lim, and K. Kikuchi, "All-optical polarization-insensitive time-division demultiplexer using a nonlinear optical loop mirror with a pair of short polarization-maintaining fibers," *IEEE Photon. Technol. Lett.*, vol. 14, pp. 1737–1739, Dec. 2002.

[11] B. Olsson and P. A. Andrekson, "Polarization-independent all-optical AND gate using randomly birefringent fiber in a nonlinear optical loop mirror," in *Proc. Optical Fiber Commun. Conf.*, Washington, DC, 1998, Optical Society of America, paper FA7.

[12] G. P. Agrawal, *Nonlinear Fiber Optics*, 3rd ed. San Diego, CA: Academic, 2001.

[13] Q. Lin and G. P. Agrawal, "Effects of polarization-mode dispersion on cross-phase modulation in dispersion-managed WDM systems," *J. Lightwave Technol.*, vol. 22, pp. 977–987, 2004.

[14] J. P. Gordon and H. Kogelnik, "PMD fundamentals: Polarization mode dispersion in optical fibers," *Proc. Nat. Acad. Sci. USA*, vol. 97, pp. 4541–4550, 2000.

[15] Q. Lin and G. P. Agrawal, "Vector theory of stimulated Raman scattering and its application to fiber-based Raman amplifiers," *J. Opt. Soc. Amer. B*, vol. 20, pp. 1616–1631, 2003.

[16] D. B. Mortimore, "Fiber loop reflectors," *J. Lightwave Technol.*, vol. 6, pp. 1217–1224, 1988.

[17] T. A. Birks and P. Morkel, "Jones calculus analysis of single-mode fiber Sagnac reflector," *Appl. Opt.*, vol. 27, pp. 3107–3113, 1988.

[18] C. Kolleck and U. Hempelmann, "All-optical wavelength conversion of NRZ and RZ signals using a nonlinear optical loop mirror," *J. Lightwave Technol.*, vol. 15, pp. 1906–1913, 1997.

[19] A. Galtarossa, L. Palmieri, M. Schiano, and T. Tambosso, "Measurement of beat length and perturbation length in long single-mode fibers," *Opt. Lett.*, vol. 25, pp. 384–386, 2000.

[20] P. K. A. Wai and C. R. Menyuk, "Polarization mode dispersion, decorrelation, and diffusion in optical fibers with randomly varying birefringence," *J. Lightwave Technol.*, vol. 14, pp. 148–157, 1996.

[21] G. J. Foschini and C. D. Poole, "Statistical theory of polarization dispersion in single mode fibers," *J. Lightwave Technol.*, vol. 9, pp. 1439–1456, 1991.

[22] M. Shtaif, A. Mecozzi, and J. A. Nagel, "Mean-square magnitude of all orders of polarization mode dispersion and the relation with the bandwidth of the principal states," *IEEE Photon. Technol. Lett.*, vol. 12, pp. 53–55, 2000.

[23] Q. Lin and G. P. Agrawal, "Impact of residual birefringence on cross-phase modulation: intrapulse depolarization in optical fibers," *Opt. Lett.*, submitted for publication.

[24] B. Olsson and P. A. Andrekson, "Polarization independent demultiplexing in a polarization diversity nonlinear optical loop mirror," *IEEE Photon. Technol. Lett.*, vol. 9, pp. 764–766, June 1997.

[25] S. J. Savage, B. S. Robinson, S. A. Hanilton, and E. P. Ippen, "All-optical pulse regeneration in an ultrafast nonlinear interferometer with Faraday mirror polarization stabilization," *Opt. Lett.*, vol. 28, pp. 13–15, 2003.

[26] J. E. Sharping, M. Fiorentino, P. Kumar, and R. S. Windeler, "All-optical switching based on cross-phase modulation in microstructure fiber," *IEEE Photon. Technol. Lett.*, vol. 14, pp. 77–79, Jan. 2002.

[27] H. Sotobayashi, C. Sawaguchi, Y. Koyamada, and W. Chujo, "Ultrfast walk-off-free nonlinear optical loop mirror by a simplified configuration for 320-Gbit/s time-division multiplexing signal demultiplexing," *Opt. Lett.*, vol. 27, pp. 1555–1557, 2002.

[28] A. Galtarossa, L. Palmieri, M. Schiano, and T. Tambosso, "Measurement of birefringence correlation length in long, single-mode fibers," *Opt. Lett.*, vol. 26, pp. 962–964, 2001.

Qiang Lin received the B.S. degree in applied physics and the M.S. degree in optics from Tsinghua University, Beijing, China, in 1996 and 1999, respectively. He is currently working toward the Ph.D. degree at the Institute of Optics, University of Rochester, Rochester, NY.

His research interest includes nonlinear fiber optics, polarization mode dispersion, optical communications, and ultrafast optics.

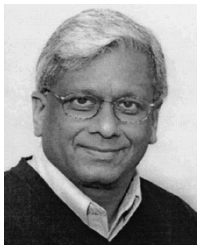

Govind P. Agrawal (M'83–SM'86–F'96) received the B.S. degree from the University of Lucknow, Lucknow, India, in 1969 and the M.S. and Ph.D. degrees from the Indian Institute of Technology, New Delhi, in 1971 and 1974, respectively.

After holding positions at the Ecole Polytechnique, Paris, France, the City University of New York, Manhattan, and AT&T Bell Laboratories, Murray Hill, NJ, he joined the Faculty of the Institute of Optics, University of Rochester, Rochester, NY, in 1989, where he is currently a Professor of optics. He is an author or coauthor of more than 300 research papers, several book chapters and review articles, and five books entitled: *Semiconductor Lasers* (Norwell, MA: Kluwer Academic, 2nd ed., 1993); *Fiber-Optic Communication Systems* (New York: Wiley, 3rd ed., 2002); *Nonlinear Fiber Optics* (San Diego, CA: Academic, 3rd ed., 2001); *Applications of Nonlinear Fiber Optics* (San Diego, CA: Academic, 2001); and *Optical Solitons: From Fibers to Photonic Crystals* (San Diego, CA: Academic, 2003). He has also edited two books: *Contemporary Nonlinear Optics* (San Diego, CA: Academic, 1992) and *Semiconductor Lasers: Past, Present and Future* (New York: AIP, 1995). He has participated multiple times in organizing technical conferences sponsored by the Optical Society of America (OSA) and the IEEE. He was the Program Cochair in 1999 and the General Cochair in 2001 for the "Quantum Electronics and Laser Science" Conference. He was a memeber of the Program committee in 2004 for the Conference on Lasers and Electro-Optics (CLEO). His research interests include optical communications, nonlinear optics, and laser physics.

Dr. Agrawal is a Fellow of the OSA.